



# Self-Densification of Highly Mesoporous Wood Structure into a Strong and Transparent Film

Kai Li, Shennan Wang, Hui Chen, Xuan Yang, Lars A. Berglund, and Qi Zhou\*

In the native wood cell wall, cellulose microfibrils are highly aligned and organized in the secondary cell wall. A new preparation strategy is developed to achieve individualization of cellulose microfibrils within the wood cell wall structure without introducing mechanical disintegration. The resulting mesoporous wood structure has a high specific surface area of  $197 \text{ m}^2 \text{ g}^{-1}$  when prepared by freeze-drying using liquid nitrogen, and  $249 \text{ m}^2 \text{ g}^{-1}$  by supercritical drying. These values are 5 to 7 times higher than conventional delignified wood ( $36 \text{ m}^2 \text{ g}^{-1}$ ) dried by supercritical drying. Such highly mesoporous structure with individualized cellulose microfibrils maintaining their natural alignment and organization can be processed into aerogels with high porosity and high compressive strength. In addition, a strong film with a tensile strength of  $449.1 \pm 21.8 \text{ MPa}$  and a Young's modulus of  $51.1 \pm 5.2 \text{ GPa}$  along the fiber direction is obtained simply by air drying owing to the self-densification of cellulose microfibrils driven by the elastocapillary forces upon water evaporation. The self-densified film also shows high optical transmittance (80%) and high optical haze (70%) with interesting biaxial light scattering behavior owing to the natural alignment of cellulose microfibrils.

interesting functionalities beyond traditional wood materials, such as transparent wood with anisotropic optical properties,<sup>[2]</sup> wood aerogel for continuous oil/water separation,<sup>[3,4]</sup> efficient solar-steam generation through wood structure,<sup>[5]</sup> densified wood composite with extraordinary specific tensile strength.<sup>[6]</sup> In preparation of these wood-based materials, delignification is an essential pretreatment step to extract lignin and partial hemicellulose, aiming to remove the chromophores, and to increase the cell wall accessibility/porosity. Further treatments such as alkaline extraction,<sup>[4]</sup> acetylation,<sup>[7]</sup> oxidation,<sup>[8,9]</sup> could be employed to control the nanostructure and surface chemistry of the delignified wood. However, although the porosity of delignified wood could reach up to 98% when low density wood species is used, typical specific surface area (SSA) for delignified wood prepared by sodium chlorite or peracetic acid delignification was between  $20\text{--}41 \text{ m}^2 \text{ g}^{-1}$ .<sup>[3,4,10]</sup> The

Wood nanotechnology has recently emerged as a promising strategy for cellulosic materials preparation through a top-down approach.<sup>[1]</sup> The multiscale hierarchy and intrinsic alignment of cellulose microfibrils in wood cell wall have inspired the fabrication of wood-based materials which outperform existing materials prepared from cellulose nanofibers (CNFs) or cellulose nanocrystals. These wood-based materials have demonstrated

SSA value for delignified wood prepared by  $\text{NaOH}/\text{Na}_2\text{SO}_3/\text{H}_2\text{O}_2$  pulping process was even below  $15 \text{ m}^2 \text{ g}^{-1}$ .<sup>[11]</sup> On the other hand, the SSA value for CNFs-based aerogels prepared via the bottom-up approach was generally in the range of  $300\text{--}600 \text{ m}^2 \text{ g}^{-1}$  when supercritical-drying was applied.<sup>[12]</sup> As a comparison, well individualized cellulose nanofiber prepared from wood pulp fibers by 2,2,6,6-tetramethylpiperidinyl-1-oxyl (TEMPO)-mediated oxidation has a uniform thickness of  $3\text{--}4 \text{ nm}$ .<sup>[13]</sup> The cellulose microfibrils in native wood cell wall mainly present in form of large fibril aggregates and the thickness of fibril aggregates also increases after the delignification process due to the removal of restricting spacers, lignin, and hemicellulose.<sup>[14]</sup> Thus, further disintegration of the fibril aggregates in the delignified wood without losing the cell wall structure and the natural alignment of cellulose microfibrils is a grand challenge in exploiting nanotechnology for wood-based materials via a top-down approach.

For cellulose nanofiber production from various cellulosic fiber resources, the individualization of cellulose microfibrils is often facilitated by the enzymatic or chemical pretreatments, for example, by using the oxidative enzyme lytic polysaccharide monooxygenase,<sup>[15]</sup> TEMPO-mediated oxidation,<sup>[13]</sup> carboxymethylation,<sup>[16]</sup> or cationization.<sup>[17]</sup> Yano et al.<sup>[18]</sup> have previously employed acetylation to avoid the fibril aggregation formed through interfibril hydrogen bonds, transforming pulp fiber to nanostructured fiber. Svensson et al.<sup>[19]</sup> performed TEMPO-mediated oxidation on both dissolving pulp and kraft pulp fibers and a highest SSA value of  $130 \text{ m}^2 \text{ g}^{-1}$  was achieved without disintegration procedure. Paper prepared from TEMPO-oxidized

Dr. K. Li, S. Wang, Prof. Q. Zhou  
Division of Glycoscience  
Department of Chemistry  
School of Engineering Sciences in Chemistry  
Biotechnology and Health  
KTH Royal Institute of Technology  
AlbaNova University Centre  
Stockholm SE-106 91, Sweden  
E-mail: qi@kth.se

Dr. K. Li, S. Wang, H. Chen, Dr. X. Yang, Prof. L. A. Berglund,  
Prof. Q. Zhou  
Wallenberg Wood Science Center  
Department of Fibre and Polymer Technology  
KTH Royal Institute of Technology  
Stockholm SE-100 44, Sweden

The ORCID identification number(s) for the author(s) of this article can be found under <https://doi.org/10.1002/adma.202003653>.

© 2020 The Authors. Published by Wiley-VCH GmbH. This is an open access article under the terms of the Creative Commons Attribution License, which permits use, distribution and reproduction in any medium, provided the original work is properly cited.

DOI: 10.1002/adma.202003653

pulp fibers were further deprotonated by sodium hydroxide to obtain enhanced tensile strength, transparency while the dewatering time was minimized to 10 s.<sup>[20]</sup> But no improvement in material properties could be concluded from the nanostructured pulp fibers as compared to CNF-based materials as the structural advantages of wood cell wall structure were lost during pulping. Li et al.<sup>[8,9]</sup> have reported the oxidation of delignified wood in TEMPO/NaClO/NaBr system at pH 10 to prepare nanofluidic cellulosic membrane. The slightly increased charge density in cellulose membrane created 2–20 nm channels between cellulose microfibrils for ion regulation. The cellulose membrane was densified to obtain tensile strength of  $58 \pm 5$  MPa which is however not comparable to TEMPO-CNF nanopaper.

Herein, we report a highly mesoporous wood structure, with fibrillated cellulose microfibrils in the cell wall, prepared by TEMPO-mediated oxidation of delignified wood at neutral condition (pH = 6.8) with TEMPO/NaClO/NaClO<sub>2</sub> system. The resulting TEMPO-oxidized wood exhibited mesoporous structure with high SSA. Aerogels prepared from the TEMPO-oxidized wood demonstrated robust compressibility and high porosity. In addition, the TEMPO-oxidized mesoporous wood in wet state could also be self-densified into thin films by drying at ambient condition without assistance of mechanical pressing or heating. The thin films showed superior mechanical properties and high optical transmittance. Different from materials assembled from nanostructured pulp fibers, the natural multi-scale alignment of cellulose microfibrils in wood cell wall was preserved after our processes, providing great possibilities in developing wood-based materials with outstanding properties.

Wood is a natural polymeric composite mainly consisting of cellulose, hemicellulose, and lignin. Balsa wood (*Ochroma pyramidale*) features intrinsic low density, thin cell wall, and small microfibril angle (MFA), which are advantageous for material preparation using wood nanotechnology.<sup>[21]</sup> After delignification of balsa wood using NaClO<sub>2</sub> at pH 4.6 and 80 °C for 12 h (Figure 1a), 1.28% residual lignin remained in the white delignified wood (Figure 1b) while cellulose and most hemicellulose were preserved. This was confirmed by wet chemical analysis (Table S1, Supporting Information) and disappearance of the peak at 1505 cm<sup>-1</sup> for aromatic ring skeleton vibration in FTIR (Figure S1, Supporting Information). NaClO<sub>2</sub> is commonly used for the preparation of holocellulose. Indeed, only a 2% loss of xylose was detected after delignification (Table S2, Supporting Information), which originated from highly substituted xylan associated with lignin.<sup>[22]</sup> The honeycomb-like cellular wood cell wall structure was well preserved after the delignification process (Figure 1c). Voids can be observed in the lignin-abundant secondary cell wall and the middle lamella owing to the removal of lignin. The delignification process increased the accessibility of cell wall and exposed the surface of cellulose fibrils for further chemical modification. In addition, a few nanosized pores and cellulose microfibrils in the form of aggregates were found in the secondary cell wall (S layer, Figure 1d,f), while the primary cell wall (P layer, Figure 1g) was still a rather dense fibrils network.

To achieve in situ fibrillation of cellulose microfibrils in bulk wood, TEMPO-mediated oxidation is considered as an efficient chemical method.<sup>[23]</sup> TEMPO-mediated oxidation features position-selective oxidation of C6-primary hydroxyl groups of

cellulose to C6-carboxylate groups. The repulsion between carboxyl groups results in fibrillation of cellulose microfibrils, which can later be reorganized into desired nanostructured materials. The system of TEMPO/NaClO/NaBr at pH 10 has been extensively used to produce CNFs with a high carboxylate content (up to 1.7 mmol g<sup>-1</sup>) and a uniform width (3–4 nm) from various resources.<sup>[24,25]</sup> Nonetheless, inevitable depolymerization of cellulose often occurs during this process. NaClO is the primary oxidant that oxidizes TEMPO to TEMPO<sup>+</sup>, which is reduced by dissociated primary hydroxyl of cellulose.<sup>[26]</sup> The latter is then oxidized to C-6 aldehyde, which can lead to  $\beta$ -alkoxy elimination in alkaline condition and depolymerization of cellulose.<sup>[13]</sup> The reduction of the molar mass of cellulose has a negative impact on the mechanical properties of CNFs based composites.<sup>[27]</sup> TEMPO-mediated oxidation of pulp fibers at weak acidic or neutral condition using the TEMPO/NaClO/NaClO<sub>2</sub> system is however different. NaClO<sub>2</sub> serves as an oxidant to oxidize any C-6 aldehyde generated by TEMPO/NaClO oxidation. Thus the formation of C-6 aldehyde and substantial depolymerization of cellulose can be avoided, and the hemicellulose content can also be preserved to some extent.<sup>[13,25,26]</sup> CNFs prepared from the neutral condition showed a carboxylate content up to 1.3 mmol g<sup>-1</sup> and longer nanofibril length as compared to those prepared by using the TEMPO/NaClO/NaBr system.<sup>[26,28]</sup>

TEMPO-oxidation in alkaline condition is efficient in hemicellulose solubilization and degradation which, on the other hand, results in removal of surface bound xylan and complete individualization of cellulose microfibrils.<sup>[25]</sup> Hence, when it was used for wood oxidation, compromise between wood structural integrity and carboxylate content had to be made, resulting in a carboxylate content reported to be 0.25 mmol g<sup>-1</sup> for oxidized wood previously.<sup>[9]</sup> In this work, TEMPO-oxidation at neutral condition was applied on delignified wood for the first time. The TEMPO-oxidized balsa wood had a carboxylate content of 0.78 mmol g<sup>-1</sup> as measured by conductimetric titration, which is three times higher than delignified balsa wood (0.26 mmol g<sup>-1</sup>) and comparable to CNFs obtained from hardwood pulp fibers.<sup>[25]</sup> Swelling of wood structure was observed in the tangential direction (Figure 1h) after TEMPO-mediated oxidation and subsequent washing with deionized water. Although the de-bonding of wood fiber cells occurred during the swelling, the structural integrity of wood remained as a microtube array structure was observed at cross section along longitudinal direction (Figure 1i). Nanoscale pores were generated in the secondary cell wall (Figure 1j), owing to the partial removal of hemicellulose and electrical repulsion between surface carboxylated cellulose microfibrils. Higher magnification scanning electron microscopy (SEM) images on the inner (S layer) and outer (P layer) surfaces of fibers in TEMPO-oxidized wood (Figure 1l and 1m, respectively) revealed the arrangement of intact cellulose microfibrils, similar to those found in native wood cell wall prepared by rapid freeze deep-etching technique.<sup>[29]</sup> The S layer (Figure 1l), which accounts up to 90% of the cell wall thickness,<sup>[30]</sup> consists of highly aligned fibrillated cellulose microfibrils with visible aggregation size of  $\approx 20$  nm. The inter-fibrillar spaces mainly presented in a double convex lens shape. The primary cell wall (Figure 1m) exhibited a random-in-plane network organization of cellulose microfibrils with a uniform size of  $\approx 10$  nm.<sup>[31]</sup>

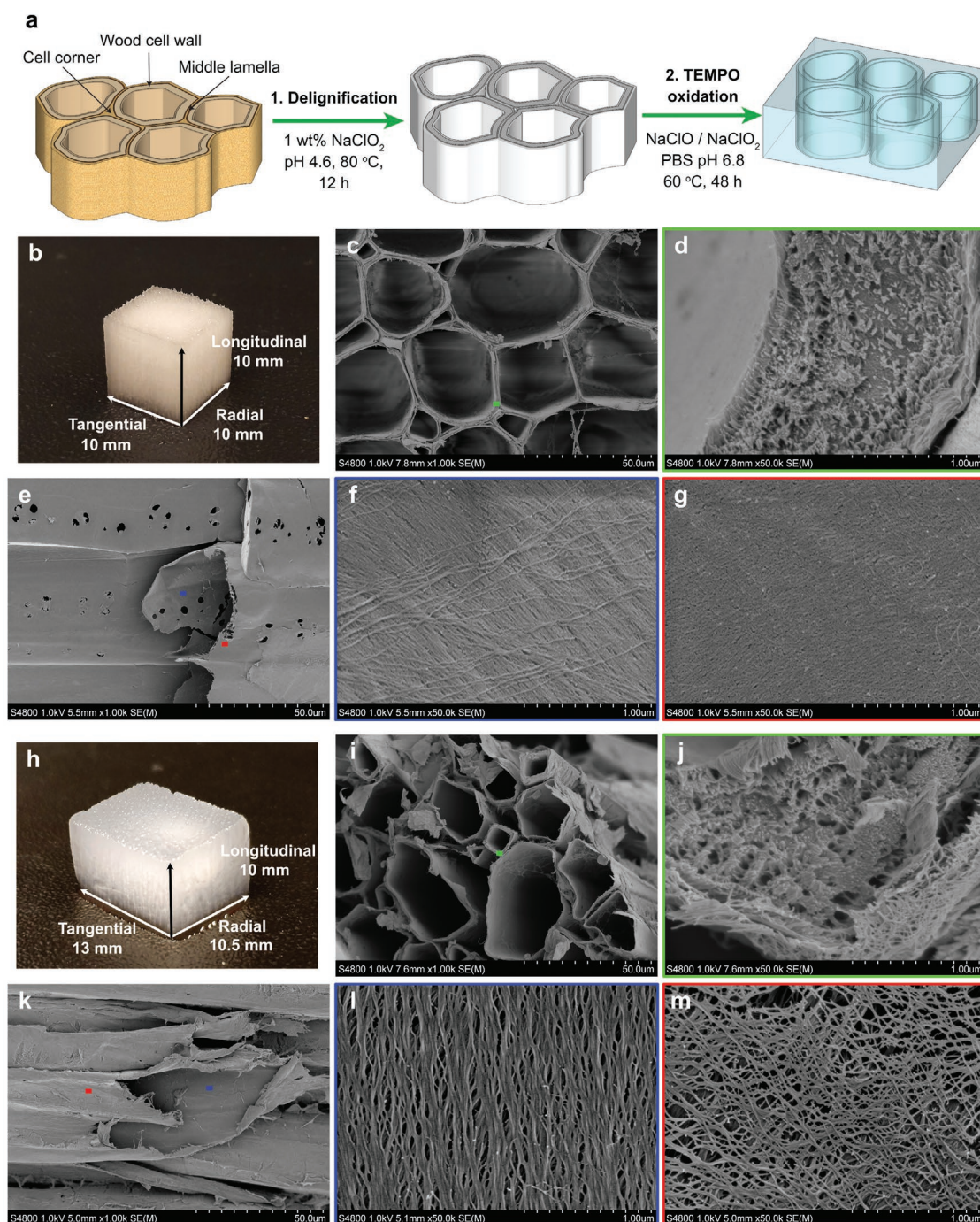


**Figure 1.** TEMPO-oxidized wood preparation and microstructure characterization. a) Schematic illustration for the two-step preparation of TEMPO-oxidized wood. b) Photograph of delignified wood. c,d) SEM images of the cross section of delignified wood. e–g) SEM images of the longitudinal section of delignified wood. h) Photograph of TEMPO-oxidized wood. i,j) SEM images of the cross section of TEMPO-oxidized wood. k–m) SEM images of longitudinal section of TEMPO-oxidized wood. Samples for SEM were prepared by freeze-drying using liquid nitrogen.

The TEMPO-oxidized wood dried by using supercritical  $\text{CO}_2$  showed a high specific surface area of  $249 \text{ m}^2 \text{ g}^{-1}$  which is over 10 times higher than the delignified wood prepared with  $\text{NaClO}_2$  and almost 20 times higher than that prepared with  $\text{NaOH}/\text{Na}_2\text{SO}_3/\text{H}_2\text{O}_2$  (Table S3, Supporting Information).<sup>[3,4,11]</sup> The SSA value of supercritical dried delignified wood prepared

in this work was  $36 \text{ m}^2 \text{ g}^{-1}$ , which is  $\approx 7$  times lower than TEMPO-oxidized wood. The drying method has a significant impact on the physical properties of wood aerogels. TEMPO-oxidized wood prepared by freeze-drying using liquid nitrogen had also a high SSA value of  $197 \text{ m}^2 \text{ g}^{-1}$ . TEMPO-oxidized wood prepared by both supercritical drying (SCD) and freeze drying

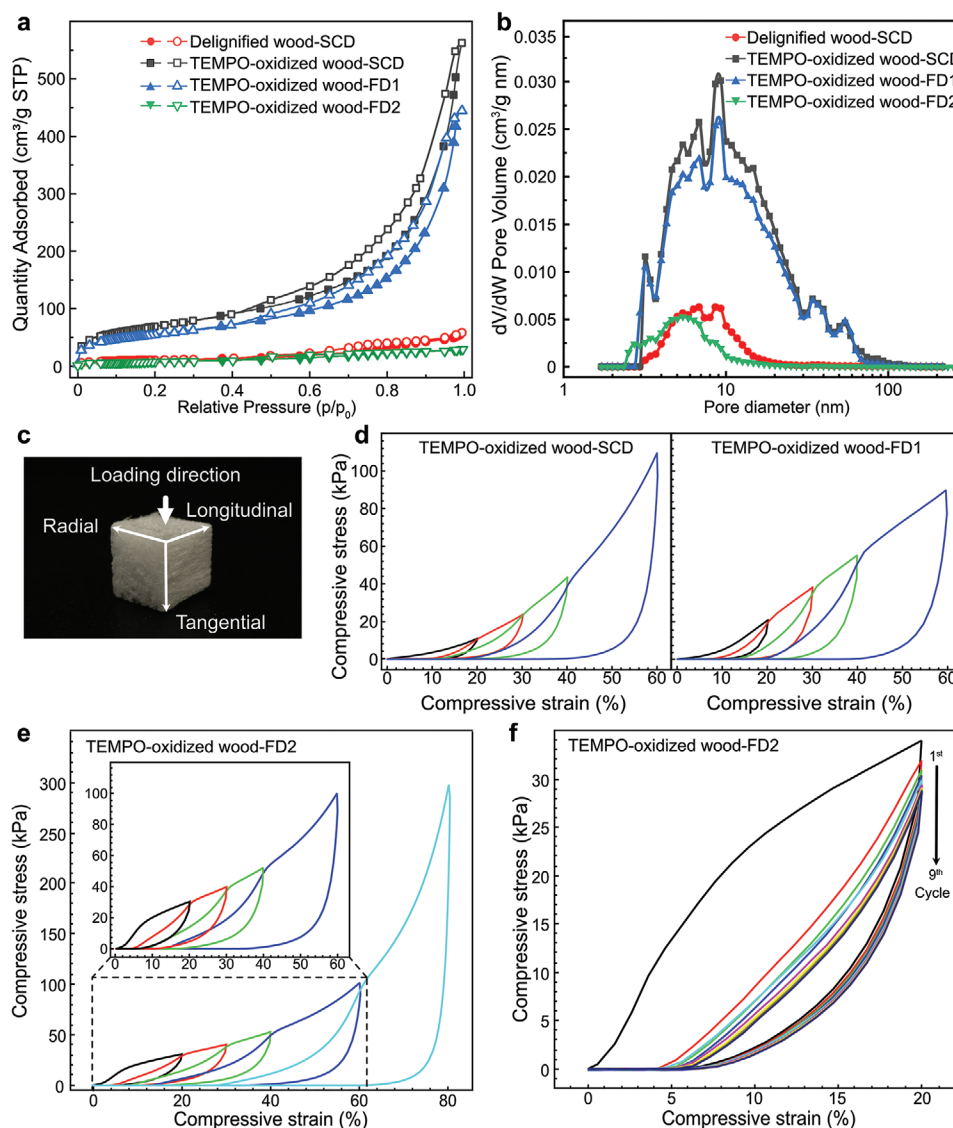


**Figure 2.** Physical properties of delignified wood and TEMPO-oxidized wood aerogels prepared by supercritical drying (SCD) and freeze-drying (FD1, rapid frozen by using liquid nitrogen; FD2, frozen in  $-20^{\circ}\text{C}$  freezer). a)  $\text{N}_2$  adsorption/desorption isotherms of delignified wood and TEMPO-oxidized wood aerogels (filled marker: adsorption isotherm, empty marker: desorption isotherm). b) Pore size distribution derived from  $\text{N}_2$  adsorption using the method of non-local density functional theory. c) Illustration of the loading direction on wood aerogels during compressive mechanical test. d) Compressive stress-strain curves with maximum strains of 20%, 30%, 40%, and 60% for TEMPO-oxidized wood aerogels (SCD and FD1). e) Compressive stress-strain curves of the TEMPO-oxidized wood aerogel (FD2) with different maximum strains of 20%, 30%, 40%, 60%, and 80%, respectively. f) Compressive stress-strain curves of the TEMPO-oxidized wood aerogel (FD2) at the maximum strain of 20% for 9 cycles.

using liquid nitrogen (FD1) showed significant higher adsorption of  $\text{N}_2$  as compared to the delignified wood (Figure 2a). Pore size distribution using the Barrett-Joyner-Halenda model is based on cylindrical pores and often used in analysis of wood pulp fiber pore structures.<sup>[32]</sup> For the ultra-structures of wood cell walls in this work, a model based on non-local density functional theory with density-independent weights and a slit-like pore geometry<sup>[33]</sup> was used to analyze the pore size distribution using nitrogen adsorption data. The results are plotted in Figure 2b and both TEMPO-oxidized wood and delignified wood show a mesoporous structure. The delignified wood had mesopores from 3 to 20 nm, while the TEMPO-oxidized wood (SCD and FD1) had mesopores from 3 to 50 nm with much

higher cumulative pore volume. Most of the pores in TEMPO-oxidized wood were in the range of 4–30 nm, same as that confirmed by the structure analysis by SEM (Figure 1i–m). However, when the TEMPO-oxidized wood was frozen at  $-20^{\circ}\text{C}$  and then lyophilized (FD2), the SSA value was  $28\text{ m}^2\text{ g}^{-1}$  and only mesopores of 2.5–10 nm were detected, corresponding to much denser cell walls as revealed by structure analysis using SEM (Figure S2, Supporting Information).

Compressive testing was conducted along the tangential direction of TEMPO-oxidized wood aerogels (Figure 2c). The compressive stress-strain curves of TEMPO-oxidized wood aerogels prepared by the SCD and FD1 methods are shown in Figure 2d. Both wood aerogels showed a linear elastic region reflecting the

cell wall bending with compressive strain up to 10%, followed by a densification region with rapid increase of the compressive stress resulting from deformation of the cell walls. The compressive stress of the FD1 aerogel at 10% strain was 5 kPa due to a rather porous cell wall structure (Figure 1i–m). The stress–strain curves of TEMPO-oxidized wood aerogel prepared by the FD2 method showed three distinct regions (Figure 2e). Particularly, as the compressive strain increased from 10% to 40%, a stress plateau stage was observed due to the gradual compression of the rather dense cell walls (Figure S2, Supporting Information), which were formed during the process of slow freezing at  $-20^{\circ}\text{C}$  and subsequent lyophilization. The compressive stress of the FD2 aerogel at 10% strain was 24 kPa, and the compressive stress at 40% strain was recorded at 52 kPa, 10 times higher than those wood aerogels previously prepared via the top–down approach.<sup>[4,11]</sup> A cyclic test at 20% strain demonstrated its good stability under multiple rounds of compression (Figure 2f). Besides, high porosity of  $96.9 \pm 0.1\%$  and low density of  $46.6 \pm 1.4\text{ kg m}^{-3}$  (Table S3, Supporting Information) was obtained for the FD2 aerogel, indicating possibility to be used for liquid absorption. Although SCD and FD1 aerogels have poorer compressibility, the low rigidity of wood cell wall provides the opportunity for better densification of the native wood structure for functional materials.

Transparent cellulose film prepared from CNFs features high mechanical toughness and optical transparency, and has been used as substrates for developing advanced electronics,<sup>[34]</sup> sensors,<sup>[35]</sup> energy storage devices,<sup>[36]</sup> and light harvesting system,<sup>[37]</sup> etc. A general approach for the film preparation involves mechanical isolation of CNFs and the self-assembly of CNFs initiated by the removal of water from dispersion through either solution casting or vacuum filtration.<sup>[23]</sup> A subsequent densification and drying process is applied to achieve high density and low porosity, which are significantly important to the improvement of mechanical strength as well as light transmittance.<sup>[38]</sup>

The TEMPO-mediated oxidation was successfully applied on delignified balsa wood with different geometry, from a large piece of wood ( $100 \times 100 \times 10\text{ mm}^3$ , Figure S3, Supporting Information) to a wood veneer ( $60 \times 30 \times 2\text{ mm}^3$ , Figure 3a). After  $\text{NaClO}_2$  delignification and TEMPO-mediated oxidation (Figure 3a), a 2 mm thick balsa wood veneer was air-dried into an 80  $\mu\text{m}$  thick transparent film on a glass plate after 24 h at ambient condition ( $22^{\circ}\text{C}$ , 30% RH) without any additional pressure. Without TEMPO-mediated oxidation, delignified wood veneer only reduced to half of its original thickness and resulted in an opaque film after drying in the same condition. The delignified wood showed insufficiently densified structure with rough surface, and apparent buckling of cell wall can be observed (Figure 3b,c). The TEMPO-oxidized wood completely collapsed into a film with layered dense structure (Figure 3d–g), which is very similar to previously reported densified wood, where external mechanical pressure and heating had to be applied.<sup>[6,39,40]</sup>

Self-densification is a solution casting process in principle, the process efficiency for TEMPO-oxidized wood film is surprisingly higher than those films casted from TEMPO-oxidized CNFs water suspension, for which several days are required at ambient condition.<sup>[41]</sup> The self-densification relies on the

elastocapillarity generated by the water flow in a flexible tube, and the water flow in the cell lumen of TEMPO-oxidized wood was driven by evaporation (Figure 3h). The water movement in wood is combined with capillary flow of free water in the cell cavities and diffusion as hygroscopic water in the cell wall and/or as water vapor through the fiber cells.<sup>[42]</sup> In natural bulk wood, capillary pressure can move the water from inside the wood to the surface and replace it with air during lumber drying process.<sup>[43]</sup> Such cavitation phenomenon takes place in xylem conduit generates negative pressure, which would lead to collapse of the tubular structure. By depositing lignin in the cell wall, tree developed resistance to collapse.<sup>[44]</sup> The native and delignified wood fibers have limited porosity. Their lumen and cell-wall micropores can be assumed as closed structure, which exhibits buckling resistance to compressive loads, that is, elastocapillary force in fiber lumen, due to the lack of flexibility.<sup>[45]</sup> TEMPO-mediated oxidation significantly increased the flexibility of wood cell wall thus there was no buckling, allowing the complete collapse of cell structure. The distance which elastocapillary force becomes effective in deforming solids is given as  $L = \gamma/E$ , where  $\gamma$  is the surface tension and  $E$  is the Young's modulus of the solid.<sup>[46]</sup> The surface tension of anisotropic surface between cellulose and pure water is  $72\text{ mN m}^{-1}$ .<sup>[47]</sup> The elastic modulus of TEMPO-oxidized wood was  $\approx 50\text{ kPa}$ . Hence the effective distance is at the magnitude of micrometers. The water content of TEMPO-oxidized wood increased from 94.5% (delignified wood) to 99.5%, indicating improved hydrophilicity and more accessible hydroxyl groups due to fibrillation. Once the two sides of lumen were in contact, strong hydrogen bonding would form between the abundant hydroxyl groups on cellulose fibrils, hence the deformation was fixed in place and high densification rate was achieved.

The self-densified film from TEMPO-oxidized balsa wood has a density of  $1.32 \pm 0.1\text{ g cm}^{-3}$ , which is the highest among the reported anisotropic densified wood films or composites (Table S4, Supporting Information) in literature.<sup>[6,39,40,48]</sup> Density is strongly correlated to the mechanical properties of materials. The in situ fibrillation of wood cell wall allows further dense packing of cellulose microfibrils during self-densification. The self-densified film showed high tensile strength of  $449.1 \pm 21.8\text{ MPa}$  and Young's modulus of  $51.1 \pm 5.2\text{ GPa}$  (Figure 3i; Table S4, Supporting Information) which are 17.3-times and 22.2-times compared to air dried delignified wood, respectively. Part of the contribution to such extraordinary mechanical properties was from the inherent alignment of cellulose microfibrils in wood cell wall. Indeed, the MFA of dominant S2 layer in balsa wood cell wall measured with wide-angle X-ray scattering was reported in the literature to be about  $1.4^{\circ}$  offset the axial direction (longitudinal direction).<sup>[21]</sup> Such high degree of orientation is still difficult to achieve for CNFs-based materials using existing artificial orientation techniques such as wet-stretching or wet-extrusion, hence the self-densification process of TEMPO-oxidized balsa wood demonstrates the advantage of preserving the natural alignment of cellulose microfibrils.<sup>[23,49]</sup> Similar mechanical performance was reported previously for densified materials from partially delignified wood<sup>[6]</sup> and alkaline-extracted delignified wood<sup>[40]</sup> (Table S4, Supporting Information). However, densification of the partially delignified wood required hot pressing for 24 h under a pressure of 5 MPa,

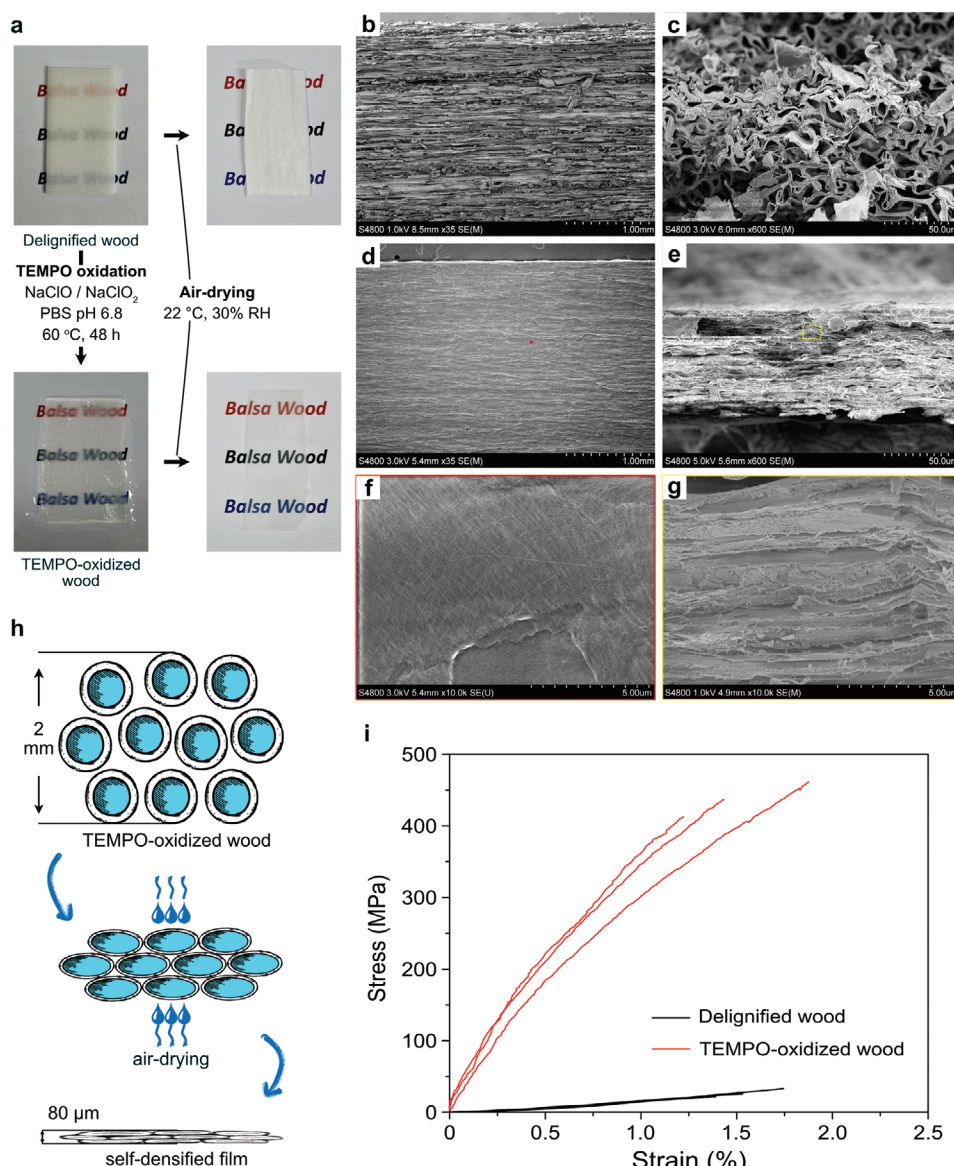


**Figure 3.** Preparation, structures, and mechanical properties of air-dried (22 °C, 30% RH) delignified wood film and TEMPO-oxidized wood film from balsa wood veneer. a) Schematic illustration for the preparation. b,c) SEM images of surface (b) and cross section (c) of air-dried delignified wood. d–g) SEM images of surface (d,f) and cross section (e,g) of the air-dried TEMPO-oxidized wood film indicating densification. h) Schematic illustration for the self-densification mechanism of the TEMPO-oxidized wood. i) Typical stress–strain curves of air-dried delignified wood and TEMPO-oxidized wood films.

and densification of the alkali-extracted delignified wood was achieved under a load of 5 kg at room temperature for up to 2 days. Our self-densified film features the highest energy efficiency in film formation processes.

Optical transparency is one of the key features for cellulose nanopaper, and has drawn a lot of attention for developing optoelectronic devices.<sup>[50]</sup> The transmittance is largely dependent on the density, thickness, and nanostructure. The self-densified film from TEMPO-oxidized balsa wood had a total optical transmittance of around 80% and a total optical haze of around 70% in the wavelength range of 400–760 nm (Figure 4a,b). As a comparison, the delignified wood dried with the same procedure had an optical transmittance of 10% (Figure S4, Supporting

Information), indicating incomplete densification. As the native alignment of cellulose microfibrils in wood cell wall was kept after TEMPO-mediated oxidation (Figure 1i), self-densified film also exhibited anisotropic light scattering behavior, similar to transparent wood/polymer composites.<sup>[39,40,51]</sup> The collected scattering light transmitted through the self-densified film showed an ellipse shape due to the different scattering intensity in orthogonal directions (Figure 3c inset), which is a key feature of anisotropic materials.<sup>[52]</sup> Detailed light intensity distributions were plotted in Figure 3c,d. Due to the alignment of cellulose microfibrils along the fiber in the longitudinal direction, light scattering perpendicular to the fiber direction had stronger intensity and wider scattering angle ( $\pm 60^\circ$ ) than that

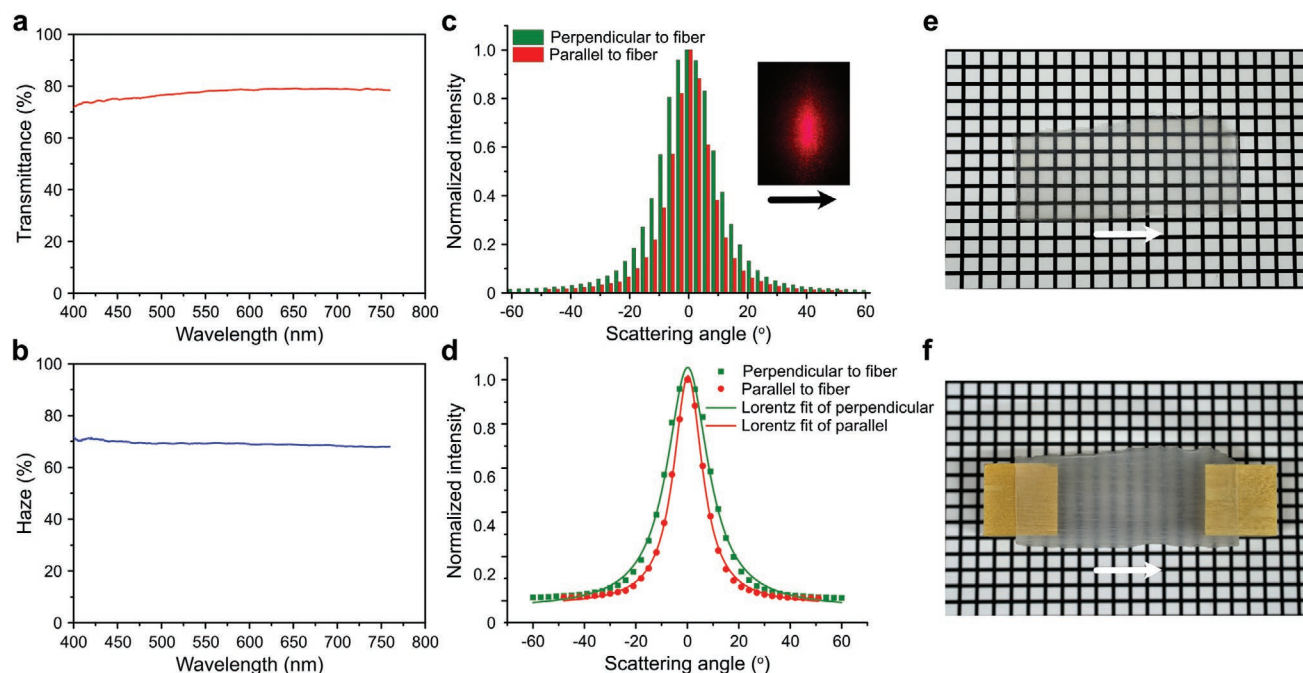


**Figure 4.** Optical properties of self-densified film from TEMPO-oxidized balsa wood. a) Optical transmittance and b) optical haze of the film (thickness = 80  $\mu\text{m}$ ). c) The normalized angular intensity distribution and d) Lorentz fit of scattered light for the film at direction perpendicular (red) and parallel (green) to fiber direction. e,f) Photographs of the film placed on a grid paper (e) and 20 mm above a grid paper (f). Arrows: fiber direction. Inset: photo of scattered light after the sample.

parallel to fiber direction ( $\pm 50^\circ$ ). When the film was placed on a grid paper, the grids could be clearly seen with no distortion (Figure 3e). As the film was leveled up to 20 mm above the grid paper, only those lines perpendicular to the microfibrils orientation could be observed with good clarity (Figure 3f).

In conclusion, TEMPO-mediated oxidation in neutral condition was successfully applied in bulk wood modification for the first time. The resulting TEMPO-oxidized wood with a carboxylate content of 0.78 mmol  $\text{g}^{-1}$  showed a highly mesoporous cell wall structure with fibrillated cellulose microfibrils and a high specific surface area of 249  $\text{m}^2 \text{g}^{-1}$  when dried by using supercritical  $\text{CO}_2$ . TEMPO-oxidized wood was processed into compressible aerogel with a high porosity of 96.9% and a low density of  $46.6 \pm 1.4 \text{ mg cm}^{-3}$  with high compressive strength by using freeze-drying technique. In addition, an interesting self-densification process was demonstrated for the fabrication of an ultrastrong transparent film at room temperature. TEMPO-mediated oxidation significantly softened the wood cell wall and allowed elastocapillary force generated by water evaporation to deform the tubular structure. The collapsed structure was further locked by hydrogen bonding between cellulose, forming a dense film with natural aligned cellulose microfibrils, which demonstrated high mechanical strength and anisotropic optical properties. Such in situ fibrillation of cellulose microfibrils enabled by TEMPO-mediated oxidation is a novel approach for cellulosic materials fabrication, taking advantages of natural wood structure. We foresee that further functionalization can be performed on TEMPO-oxidized wood to form multifunctional materials with the interests from flexible electronics, strain sensing, environmental remediation, etc.

## Experimental Section

**Materials and Chemicals:** Balsa wood (*O. pyramidale*) was purchased from Wentzel's Co. Ltd., Sweden. According to different demonstrations purposes, balsa wood was cut into dimension of  $10 \times 10 \times 10 \text{ mm}^3$  or  $60 \times 30 \times 2 \text{ mm}^3$  (longitudinal  $\times$  radial  $\times$  tangential). The oven dry density and equilibrium moisture content at RH 30% of balsa wood were  $112 \pm 5 \text{ mg cm}^{-3}$  and  $5.01 \pm 0.35\%$  respectively. Sodium chlorite ( $\text{NaClO}_2$ , 80%), sodium hypochlorite ( $\text{NaClO}$ ), sodium phosphate, and 2,2,6,6-tetramethyl-1-piperidinyloxy were purchased from Sigma-Aldrich, Germany.

**Chemical Treatment:** The wood samples were delignified using 1 wt% of sodium chlorite with acetate buffer (pH 4.6) at  $80^\circ\text{C}$  for 12 h. After delignification, samples were washed thoroughly with deionized water. The delignified balsa wood (dry mass of 1 g) was immersed in 0.1 M sodium phosphate (PBS) solvent (200 mL, pH 6.8) dissolving TEMPO (0.032 g, 0.2 mmol) and sodium chlorite (2.26 g) in a sealed beaker. 20 mL 0.1 M sodium hypochlorite PBS solution was added into the beaker. The beaker was placed at RT overnight and reaction was then carried out at  $60^\circ\text{C}$  for 48 h without stirring to avoid mechanical disintegration. The TEMPO-oxidized wood was washed with deionized water until the swelling stopped.

**Self-Densified Film and Compressible Aerogel:** The TEMPO-oxidized wood samples with  $60 \times 30 \times 2 \text{ mm}^3$  starting dimension were gently transferred onto a glass plate and left at ambient temperature ( $22^\circ\text{C}$ , 30% RH) for 24 h to form self-densified film. The TEMPO-oxidized wood samples with  $10 \times 10 \times 10 \text{ mm}^3$  was rapidly frozen in liquid nitrogen ( $-196^\circ\text{C}$ ) or at  $-20^\circ\text{C}$  overnight and then lyophilized to form aerogels. Delignified wood and TEMPO-oxidized wood were also solvent exchanged to ethanol and dried with supercritical  $\text{CO}_2$  for  $\text{N}_2$  gas adsorption test and compressive test.

**Measurements and Characterizations:** The morphologies of different wood samples were imaged with a scanning electron microscope (S-4800, Hitachi, Japan). Both tensile and compressive test were performed on a universal testing machine (Instron 5944, UK) at ambient condition ( $25^\circ\text{C}$  and 50% RH). For tensile test, the sample strips with

dimension of 50 mm × 5 mm (longitudinal × radial) was stretched at a tension speed of 1 mm min<sup>-1</sup>. Compressive test upon TEMPO-oxidized wood aerogels was conducted at a strain rate of 5% min<sup>-1</sup>, with a 500 N load cell. Prior to N<sub>2</sub> gas adsorption test, samples dried with supercritical CO<sub>2</sub> or freeze-drying were degassed at 50 °C for 48 h. N<sub>2</sub> adsorption and desorption isotherms were obtained at 77 K with a 3Flex instrument (Micromeritics Instrument Corp., Norcross, GA, USA) at the relative pressures in the range of 0.01–0.995.

**Haze and Transmittance Test:** The optical transmittance of wood film was measured using an integration sphere. First, the white (W) and dark (D) reference were measured with the incident beam going into the integration sphere or turned off. Then the sample was placed in front of the integration sphere and the transmittance was obtained. Haze was measured based on the ASTM D1003 “Standard Method for Haze and Luminous Transmittance of Transparent Plastics”, which is described as

$$\text{Haze} = \left( \frac{T_4}{T_2} - \frac{T_3}{T_1} \right) \times 100\% \quad (1)$$

where T<sub>1</sub>, T<sub>2</sub>, T<sub>3</sub>, and T<sub>4</sub> were measured according to ref. [52].

A He–Ne laser (633nm) with a beam size 3 mm was passed through the sample, then a power meter was placed on a rotation stage with the radius of 13.6 cm, and the moving step was 3° horizontally. To investigate the scattering property along and perpendicular to the fiber direction, the sample was placed with the fiber direction both parallel and perpendicular to the rotation stage where a detector/power meter was placed.

## Supporting Information

Supporting Information is available from the Wiley Online Library or from the author.

## Acknowledgements

K.L. and S.W. contributed equally to this work. The authors thank Wallenberg Wood Science Centre (WWSC) and the Swedish Foundation for International Cooperation in Research and Higher Education STINT (CH2017-7275) for supporting this work. S.W. thanks the China Scholarship Council (CSC) for supporting his Ph.D. study. X.Y., H.C., and L.B. acknowledge funding from European Research Council (ERC), Grant agreement no. 742733. The authors are grateful to Salla Koskela for illustration of Figure 3h.

## Conflict of Interest

The authors declare no conflict of interest.

## Keywords

aerogel, mechanical properties, oxidation, transparent film, wood

Received: May 28, 2020

Revised: August 1, 2020

Published online: September 2, 2020

[1] C. J. Chen, Y. D. Kuang, S. Z. Zhu, I. Burgert, T. Keplinger, A. Gong, T. Li, L. Berglund, S. J. Eichhorn, L. B. Hu, *Nat. Rev. Mater.* **2020**, <https://doi.org/10.1038/s41578-020-0195-z>.

[2] a) Y. Li, Q. Fu, S. Yu, M. Yan, L. Berglund, *Biomacromolecules* **2016**, *17*, 1358; b) M. Zhu, J. Song, T. Li, A. Gong, Y. Wang, J. Dai, Y. Yao, W. Luo, D. Henderson, L. Hu, *Adv. Mater.* **2016**, *28*, 5181.

- [3] Q. Fu, F. Ansari, Q. Zhou, L. A. Berglund, *ACS Nano* **2018**, *12*, 2222.
- [4] H. Guan, Z. Y. Cheng, X. Q. Wang, *ACS Nano* **2018**, *12*, 10365.
- [5] C. Chen, Y. Li, J. Song, Z. Yang, Y. Kuang, E. Hitz, C. Jia, A. Gong, F. Jiang, J. Y. Zhu, B. Yang, J. Xie, L. Hu, *Adv. Mater.* **2017**, *29*, 1701756.
- [6] J. W. Song, C. J. Chen, S. Z. Zhu, M. W. Zhu, J. Q. Dai, U. Ray, Y. J. Li, Y. D. Kuang, Y. F. Li, N. Quispe, Y. G. Yao, A. Gong, U. H. Leiste, H. A. Bruck, J. Y. Zhu, A. Vellore, H. Li, M. L. Minus, Z. Jia, A. Martini, T. Li, L. B. Hu, *Nature* **2018**, *554*, 224.
- [7] Y. Y. Li, X. Yang, Q. L. Fu, R. Rojas, M. Yan, L. Berglund, *J. Mater. Chem. A* **2018**, *6*, 1094.
- [8] T. Li, S. X. Li, W. Kong, C. Chen, E. Hitz, C. Jia, J. Dai, X. Zhang, R. Briber, Z. Siwy, M. Reed, L. Hu, *Sci. Adv.* **2019**, *5*, eaau4238.
- [9] T. Li, X. Zhang, S. D. Lacey, R. Mi, X. Zhao, F. Jiang, J. Song, Z. Liu, G. Chen, J. Dai, Y. Yao, S. Das, R. Yang, R. M. Briber, L. Hu, *Nat. Mater.* **2019**, *18*, 608.
- [10] Q. Fu, L. Medina, Y. Li, F. Carosio, A. Hajian, L. A. Berglund, *ACS Appl. Mater. Interfaces* **2017**, *9*, 36154.
- [11] J. Song, C. Chen, Z. Yang, Y. Kuang, T. Li, Y. Li, H. Huang, I. Kierzewski, B. Liu, S. He, T. Gao, S. U. Yurker, A. Gong, B. Yang, L. Hu, *ACS Nano* **2018**, *12*, 140.
- [12] a) H. Sehaqui, Q. Zhou, O. Ikkala, L. A. Berglund, *Biomacromolecules* **2011**, *12*, 3638; b) Y. Kobayashi, T. Saito, A. Isogai, *Angew. Chem., Int. Ed.* **2014**, *53*, 10394.
- [13] A. Isogai, T. Saito, H. Fukuzumi, *Nanoscale* **2011**, *3*, 71.
- [14] L. Salmén, *Ann. For. Sci.* **2015**, *72*, 679.
- [15] S. Koskela, S. N. Wang, D. F. Xu, X. Yang, K. Li, L. A. Berglund, L. S. McKee, V. Bulone, Q. Zhou, *Green Chem.* **2019**, *21*, 5924.
- [16] L. Wagberg, G. Decher, M. Norgren, T. Lindstrom, M. Ankerfors, K. Axnas, *Langmuir* **2008**, *24*, 784.
- [17] A. Pei, N. Butchosa, L. A. Berglund, Q. Zhou, *Soft Matter* **2013**, *9*, 2047.
- [18] H. Yano, S. Sasaki, M. I. Shams, K. Abe, T. Date, *Adv. Opt. Mater.* **2014**, *2*, 231.
- [19] A. Svensson, P. T. Larsson, G. Salazar-Alvarez, L. Wagberg, *Carbohydr. Polym.* **2013**, *92*, 775.
- [20] Y. C. Gorur, P. A. Larsson, L. Wagberg, *Biomacromolecules* **2020**, *21*, 1480.
- [21] M. Borrega, P. Ahvenainen, R. Serimaa, L. Gibson, *Wood Sci. Technol.* **2015**, *49*, 403.
- [22] L. Salmen, I. Burgert, *Holzforschung* **2009**, *63*, 121.
- [23] A. J. Benítez, A. Walther, *J. Mater. Chem. A* **2017**, *5*, 16003.
- [24] a) T. Saito, Y. Nishiyama, J. L. Putaux, M. Vignon, A. Isogai, *Biomacromolecules* **2006**, *7*, 1687; b) Y. Fan, T. Saito, A. Isogai, *Carbohydr. Polym.* **2009**, *77*, 832; c) Y. Okita, T. Saito, A. Isogai, *Biomacromolecules* **2010**, *11*, 1696.
- [25] R. Kuramae, T. Saito, A. Isogai, *React. Funct. Polym.* **2014**, *85*, 126.
- [26] T. Saito, M. Hirota, N. Tamura, H. Fukuzumi, L. Heux, A. Isogai, *Biomacromolecules* **2009**, *10*, 1992.
- [27] Z. Fang, B. Li, Y. Liu, J. Zhu, G. Li, G. Hou, J. Zhou, X. Qiu, *Matter* **2020**, *2*, 1000.
- [28] a) A. Isogai, T. Hänninen, S. Fujisawa, T. Saito, *Prog. Polym. Sci.* **2018**, *86*, 122; b) R. Tanaka, T. Saito, A. Isogai, *Int. J. Biol. Macromol.* **2012**, *51*, 228; c) T. Saito, M. Hirota, N. Tamura, A. Isogai, *J. Wood Sci.* **2010**, *56*, 227.
- [29] G. Daniel, in *Secondary Xylem Biology*, Academic Press, London, UK **2016**, p. 309.
- [30] M. Borrega, L. J. Gibson, *Mech. Mater.* **2015**, *84*, 75.
- [31] I. Burgert, P. Fratzl, *Integr. Comp. Biol.* **2009**, *49*, 69.
- [32] M. Kimura, Z.-D. Qi, A. Isogai, *Nord. Pulp Pap. Res. J.* **2016**, *31*, 198.
- [33] a) J. Shi, S. Avramidis, *Wood Sci. Technol.* **2018**, *52*, 1025; b) J. Yin, K. Song, Y. Lu, G. Zhao, Y. Yin, *Wood Sci. Technol.* **2015**, *49*, 987.
- [34] Y. Fujisaki, H. Koga, Y. Nakajima, M. Nakata, H. Tsuji, T. Yamamoto, T. Kurita, M. Nogi, N. Shimidzu, *Adv. Funct. Mater.* **2014**, *24*, 1657.

- [35] C. Yan, J. Wang, W. Kang, M. Cui, X. Wang, C. Y. Foo, K. J. Chee, P. S. Lee, *Adv. Mater.* **2014**, 26, 2022.
- [36] S. Zhou, X. Kong, B. Zheng, F. Huo, M. Stromme, C. Xu, *ACS Nano* **2019**, 13, 9578.
- [37] Z. Fang, H. Zhu, Y. Yuan, D. Ha, S. Zhu, C. Preston, Q. Chen, Y. Li, X. Han, S. Lee, G. Chen, T. Li, J. Munday, J. Huang, L. Hu, *Nano Lett.* **2014**, 14, 765.
- [38] H. L. Zhu, Z. Q. Fang, C. Preston, Y. Y. Li, L. B. Hu, *Energy Environ. Sci.* **2014**, 7, 269.
- [39] M. Zhu, Y. Wang, S. Zhu, L. Xu, C. Jia, J. Dai, J. Song, Y. Yao, Y. Wang, Y. Li, D. Henderson, W. Luo, H. Li, M. L. Minus, T. Li, L. Hu, *Adv. Mater.* **2017**, 29, 1606284.
- [40] Q. Fu, Y. Chen, M. Sorieul, *ACS Nano* **2020**, 14, 3528.
- [41] M. Zhao, F. Ansari, M. Takeuchi, M. Shimizu, T. Saito, L. A. Berglund, A. Isogai, *New Horiz.* **2018**, 3, 28.
- [42] E. T. Engelund, L. G. Thygesen, S. Svensson, C. A. S. Hill, *Wood Sci. Technol.* **2012**, 47, 141.
- [43] L. Wadsö, *Capillarity in Wood and Related Concepts : A Critical Review*, Report TVBM, Vol. 3069, Division of Building Materials, Lund University, Sweden **1995**.
- [44] a) U. G. Hacke, J. S. Sperry, W. T. Pockman, S. D. Davis, K. A. McCulloh, *Oecologia* **2001**, 126, 457; b) M. D. Venturas, J. S. Sperry, U. G. Hacke, *J. Integr. Plant Biol.* **2017**, 59, 356.
- [45] a) A. Akbari, R. J. Hill, T. G. van de Ven, *Proc. Math. Phys. Eng. Sci.* **2015**, 471, 20150184; b) T. B. Hoberg, E. Verneuil, A. E. Hosoi, *Phys. Fluids* **2014**, 26, 122103.
- [46] a) J. Bico, E. Reyssat, B. Roman, *Ann. Rev. Fluid Mech.* **2018**, 50, 629; b) R. W. Style, R. Boltyskiy, B. Allen, K. E. Jensen, H. P. Foote, J. S. Wettlaufer, E. R. Dufresne, *Nat. Phys.* **2014**, 11, 82.
- [47] A. F. Miller, A. M. Donald, *Langmuir* **2002**, 18, 10155.
- [48] a) C.-H. Fang, N. Mariotti, A. Cloutier, A. Koubaa, P. Blanchet, *Eur. J. Wood Wood Prod.* **2011**, 70, 155; b) M. Frey, D. Widner, J. S. Segmehl, K. Casdorff, T. Keplinger, I. Burgert, *ACS Appl. Mater. Interfaces* **2018**, 10, 5030; c) W. Gan, C. Chen, H. T. Kim, Z. Lin, J. Dai, Z. Dong, Z. Zhou, W. Ping, S. He, S. Xiao, M. Yu, L. Hu, *Nat. Commun.* **2019**, 10, 5084; d) X. Han, Y. Ye, F. Lam, J. Pu, F. Jiang, *J. Mater. Chem. A* **2019**, 7, 27023.
- [49] a) H. Sehaqui, N. Ezekiel Mushi, S. Morimune, M. Salajkova, T. Nishino, L. A. Berglund, *ACS Appl. Mater. Interfaces* **2012**, 4, 1043; b) S. Iwamoto, A. Isogai, T. Iwata, *Biomacromolecules* **2011**, 12, 831; c) K. M. Hakansson, A. B. Fall, F. Lundell, S. Yu, C. Krywka, S. V. Roth, G. Santoro, M. Kvik, L. Prahl Wittberg, L. Wagberg, L. D. Soderberg, *Nat. Commun.* **2014**, 5, 4018; d) C. Baez, J. Considine, R. Rowlands, *Cellulose* **2014**, 21, 347.
- [50] a) M. Nogi, S. Iwamoto, A. N. Nakagaito, H. Yano, *Adv. Mater.* **2009**, 21, 1595; b) D. Ha, N. B. Zhitenev, Z. Fang, *Adv. Electron. Mater.* **2018**, 4, 1870025.
- [51] Y. Li, S. Yu, J. G. C. Veinot, J. Linnros, L. Berglund, I. Sychugov, *Adv. Opt. Mater.* **2017**, 5, 1600834.
- [52] E. Vasileva, H. Chen, Y. Li, I. Sychugov, M. Yan, L. Berglund, S. Popov, *Adv. Opt. Mater.* **2018**, 6, 1800999.